

A Quinone-bromide Flow Battery with 1 W/cm² Power Density

Qing Chen, Michael R. Gerhardt, Lauren Hartle, Michael J. Aziz*

Harvard School of Engineering and Applied Sciences, Cambridge, MA 02138

* E-mail: maziz@harvard.edu

Abstract

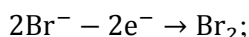
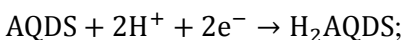
We report the performance of a quinone-bromide redox flow battery and its dependence on electrolyte composition, flow rate, operating temperature, electrode and membrane materials and pre-treatment. The results of this study are used to develop a cell with a peak galvanic power density reaching 1.0 W/cm².

Introduction

Redox flow batteries (RFBs) are promising candidates for the integration of intermittent renewable power sources with the power grid due to their potential for high safety and long discharge duration at low cost.¹⁻⁵ The most technologically mature system – the vanadium RFB -- has now reached a peak power density of 1.34 W/cm²,⁶ but the high price of vanadium sets a high floor on the system cost per kWh. Redox-active organics in aqueous solution have received recent attention due to their high performance and low cost,⁷⁻⁹ with initial reports of peak galvanic power densities reaching 0.6 W/cm² in non-optimized cells⁷. Here we study the performance of a quinone-bromide flow battery (QBFB) and its dependence on electrolyte composition, flow rate, operating temperature, electrode and membrane materials and pre-treatment of these materials. The results of this study are used to raise the peak galvanic power density to 1.0 W/cm².

Experimental

The cell design (Fig. 1) is based on that in Ref. 7. On each side, a commercial graphite plate with interdigitated flow channels¹⁰ (Fuel Cell Tech, Albuquerque, NM) was used to feed electrolyte to a porous carbon paper electrode at a rate controlled by a MasterFlex (Cole Parmer) diaphragm pump. The temperature of the cell was controlled by heating tapes from 20 to 45 °C, a range anticipated to be encountered in normal operation. The electrode comprised a stack of 6 sheets of Toray 060 (each nominally 200 μm thick), or 3 sheets of SGL 10AA (each nominally 400 μm thick) carbon paper, compressed to ~75% of the original thickness, defined by Teflon gaskets. The geometric area of the electrodes was 2 cm². No electrocatalyst was added to the carbon papers. The Toray paper was pre-treated, first by sonication in isopropanol, and then by etching in a 1:3 (v/v) mixture of concentrated nitric and sulfuric acids at 50 °C for 5 hours. The SGL paper was pre-treated by baking at 400 °C in air for 24 hours. The two papers were pre-treated differently because we noticed that the same etching protocol caused significant damage to the SGL paper which subsequently fractured upon handling. A Nafion membrane of variable thickness served as the ion-selective membrane. Its pre-treatment consisted of heating in DI water at 85 °C for 15 min., followed by soaking in 5% hydrogen peroxide for 30 min., and then by soaking in 0.05 M H₂SO₄ for 1 hour. Assembled fully discharged, the negative electrolyte ("negolyte") (20 mL) contained 1 M 9,10-anthraquinone-2,7-disulfonic acid (AQDS), ion exchanged from its sodium salt (TCI) and 1 M H₂SO₄, and the positive electrolyte ("posolyte") (24 mL) contained 3 or 3.5 M hydrobromic acid and 0.5 or 2 M Br₂. The nominal reactions during the charging process on each side are as follows:



they are reversed during discharging. In actuality, molecular complexation among oxidized and reduced species at high concentrations on each side complicates the chemistry somewhat. This complexation is currently under study and is neglected for the purpose of the present work.

We compare the effects of configuration changes to a base case configuration. It consists of pre-treated SGL electrodes, 200 mL/min. flow rates, a pre-treated Nafion 212 membrane (50 μm), and 20 $^{\circ}\text{C}$ cell temperature, with 3 M HBr and 0.5 M Br_2 in the posolyte. We provide an excess of posolyte chemicals in order to more fully interrogate the performance of the negolyte chemicals. Therefore the cell state of charge (SOC) is defined as the state of charge of the negolyte, i.e. the ratio of instantaneous nominal hydroquinone concentration to the total quinone + hydroquinone concentration (1 M). Electrochemical tests were carried out by a Gamry 30k booster connected to a Gamry Reference 3000 potentiostat. Polarization curves were recorded by measuring the current during linear sweeping at a rate of 100 mV/s. We find that this method yields the same relationship between voltage and current density as do potentiostatic or galvanostatic holding tests in our experimental setup, but without significantly changing the SOC of the relatively small volume of electrolytes used in the tests. To reach to a specific SOC, a charge threshold, derived from the charge capacity measured in the first cycle, was set during a potentiostatic charging process (at 1.3 V). Area-specific resistance (ASR) values were evaluated from electrochemical impedance spectroscopy (EIS) at high AC frequency (~ 100 kHz).

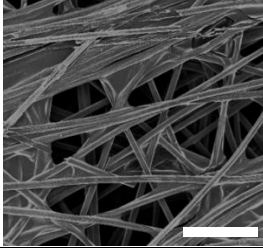
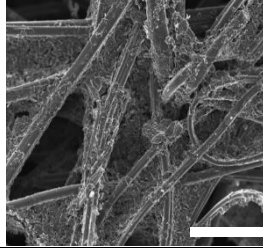
We employ the commonly-used simple method of evaluating early-stage cell performance through measuring polarization, i.e. the relationship between voltage and current density. More complicated evaluation, e.g. cycling behavior, is the subject of ongoing work. Previous research on the QBFB indicates that the polarization curves are essentially linear, except when reactant mass transport limitations become important (discharging at low SOC or charging at high SOC)⁷. This is also confirmed in our base case as shown by Fig. 1b. Therefore, for simplicity, we focus on the parametric dependencies of the polarization curve at 50% SOC.

Results and Discussion

Electrode manufacturer and pre-treatment. We start by comparing the porous carbon electrodes, varying the manufacturer and pre-treatment. Electrode properties of the Toray and SGL carbon paper are tabulated in Table 1. In the comparison test, the overall electrode thickness was kept the same for each side (i.e. 6 sheets of Toray vs. 3 sheets of SGL at a nominal thickness of 2400 μm). In Fig. 2a we show the polarization curves for various electrodes. With the exception of the untreated Toray, all curves show essentially linear behavior, characterized by an open-circuit voltage (OCV) of 0.80 volts and a slope of the polarization curve — which we term the polarization resistance and denote by r_{pol} (with units of $\text{m}\Omega\text{cm}^2$) — that is reasonably independent of current density but varies with electrode manufacturer and treatment. As shown in Fig. 2a, the SGL paper exhibits a significantly lower value of r_{pol} than the Toray paper, and both electrodes benefit from their pre-treatments. These results agree with literature reports on other RFB systems.^{10,11} We hypothesized that the difference in electrode performance may originate mainly from two characteristics: active surface area and through-plane ASR. The area-specific resistance of the four tested electrodes, r_{dry} , was evaluated by direct DC measurements in a dry cell (the same flow cell, but without electrolytes and membrane). The measured r_{dry} values are plotted against the overall uncompressed thickness in Fig. 2c. The measured r_{dry} values do not vary strongly with manufacturer or pre-treatment with the exception of the etched Toray. The higher resistance of etched Toray might be caused by destruction of carbon fibers or by the formation of a thick layer of surface oxide from the harsh pretreatment.¹² Its value at the 2400 μm (six sheets on each side, corresponding to the configuration in Fig. 2a) exceeds 80 $\text{m}\Omega\text{cm}^2$, accounting for approximately 20% of the r_{pol} (~ 437 $\text{m}\Omega\text{cm}^2$). The observation

that etching Toray reduces its value of r_{pol} but greatly raises its value of r_{dry} indicates that electrode resistance is not an important determining factor for the ASR under the conditions studied.

Table 1. Electrode property comparison. All information is provided by the vendor’s data sheet (Fuel Cell Tech), except the micrographs.

	Toray 060	SGL 10AA
Thickness/ μm	~200	~400
Porosity	0.78	0.82
Through-plane ASR/ $\text{m}\Omega\text{cm}^2$	1.6	<16
Micro-structure (Scanning electron micrographs; scale bars: 100 μm)		

The main difference contributing to the different performance is therefore presumed to be the active surface area. A simple order-of-magnitude calculation indicates that the majority of the surface of the untreated Toray is electrochemically inactive. The exchange current density, i_0 , for bromine/bromide -- the more sluggish of the two couples -- can be estimated by

$$i_0 = k_{Br} F (a_{Br_2})^\alpha (0.5 a_{Br^-})^{1-\alpha} \quad (1)$$

where F is the Faraday constant (96485 C/mol), a_j is the activity of species j (which is assumed to be its starting concentration) and α is the charge transfer coefficient. Given a kinetic rate constant (k_{Br}) of $5.8 \times 10^{-4} \text{ cm/s}^{13}$ and assuming $\alpha = 0.5$, Eq. 1 leads to an exchange current density of 50 A/cm^2 . Both experiments and theoretical calculation¹¹ have indicated that the Toray paper has a specific area of $\sim 200 \text{ cm}^{-1}$. This corresponds to about 24 cm^2 carbon surface per cm^2 geometric electrode area in each six-layer side of our cell. Thus our cell should attain an exchange current per unit geometric area of $1,200 \text{ A/cm}^2$, which is three orders of magnitude higher than the short-circuit current densities reported in Fig. 1a. In contrast, the noticeable curvature of the polarization curve for untreated Toray indicates a substantial kinetic overvoltage, which can occur only at a significant fraction of the actual exchange current density. This contrast implies that a majority of the surface couldn’t be accessed. This inference is supported by the lack of wetting behavior of the untreated Toray illustrated in Fig. 2b.

The SGL paper has the same wetting issue (Fig. 2b) despite its presumably higher specific area supplied by particulate carbon (see micrograph in Table 1). Both pretreatments help mitigate this problem through improved hydrophilicity, as demonstrated in Fig. 2b. The pre-treated carbon paper allows water permeation whereas water stays atop the untreated paper after the same period of testing time. In addition to the surface area and resistance effects, we note that recent work by Pour *et al*¹⁴ points out that pre-treatment can functionalize graphene plane edges, thereby affording catalytic benefits.

Membrane thickness and pre-treatment. The Nafion membrane behaves like a resistor in the cell, the value of which can be affected by membrane thickness and a pretreatment that opens up ion passages. Fig. 3a compares the results from cells using Nafion 115 (125 μm), 212 (50 μm) and pre-treated 212. The performance enhancement is in line with decreasing membrane resistance. We measured the cell ASR via EIS, and the real values at high frequency (r_{hr}) include membrane and electrode resistances. i_{hr} -correction

of the curves in Fig. 3a by subtracting ir_{hf} from the measured overvoltage yields polarization curves without overvoltage contributions from membrane and electrode resistance, as shown in Fig. 3b. The adjusted curves overlay with each other fairly well, indicating that membrane resistance can explain the different performance among the three tested membranes.

Flow rate. Figure 3c shows the effect of negolyte flow rate. Raising the rate above 100 mL/min seems to yield insignificant changes, whereas slower flow produces noticeable changes. When the flow rate is reduced to 50 mL/min, the value of r_{pol} gets larger, but the polarization curve remains linear, which is unexpected when mass transport limitation becomes important. We note similar observations have been made in vanadium RFB¹⁰. This could come from redistribution of the reaction zone inside the porous electrode leading to different electrolyte resistance contribution. Further investigation is underway to understand this behavior.

Operating temperature. While elevated temperatures arise from energy losses during normal battery operation, higher cell temperature leads to higher current density at a fixed voltage (Fig. 3d), as one would expect from several mechanisms. r_{pol} decreases from 323 to 247 mΩcm² as the temperature increases from 20 to 40 °C. The membrane resistance over this same temperature range drops from 61 to 50 mΩcm², which accounts for only a small fraction of the drop in r_{pol} . We attribute the remainder to the combined effects of temperature on redox rate constant, reactant diffusivity, and electrolyte conductivity.

Posolyte composition. At last, we have also tuned the posolyte content with the purpose of achieving a higher cell voltage. Lowering the HBr concentration or increasing the Br₂ concentration should increase the posolyte redox potential and thereby increase the cell voltage, according to the Nernst equation,

$$E_{\text{pos}} = E^0_{\text{Br}_2/\text{Br}^-} + \frac{RT}{nF} \ln \left(\frac{a_{\text{Br}_2}}{a_{\text{Br}^-}{}^2} \right) \quad (2)$$

where $E^0_{\text{Br}_2/\text{Br}^-}$ is the standard redox potential of the bromine/bromide couple, R is the gas constant, n is the charge transfer number and T is the temperature in Kelvin. Although complexation and non-ideal solution behavior complicate the prediction of activities from species concentrations, we expect a monotonically increasing, if not strictly proportional, relationship between these two properties. We show in Fig. 4 that the two proposed approaches do indeed lead toward higher open-circuit voltage. A drawback of significantly lowering the HBr concentration is an increase in membrane and electrolyte resistance; thus, we avoided large cuts to the posolyte bromide concentration.

High power density cell. Based on the understanding developed from the work described above, we changed the configuration of the QBFB to raise the power output. Baked SGL paper was used for the electrodes, with a pre-treated Nafion 212 membrane separating the two sides. 2 M Br₂ was added to the 3 M HBr posolyte in the fully discharged state. No change was made to the negolyte. The cell operated at 40 °C, and the negolyte flow rate was 400 mL/min. These modifications significantly boost the cell current and power outputs, as shown by the polarization and power curves in Fig. 5. At 90% SOC, the short-circuit current density exceeds 4 A/cm² and the peak power density reaches 1.0 W/cm², which is a significant boost compared to the base case (dashed lines in Fig. 5b). We note that despite the high power output, we expect a high rate of bromine cross-over, resulting from both the high Br₂ content of the posolyte and the membrane pre-treatment. Managing such crossover is the subject of ongoing work.

In summary, we have characterized the effects of several factors on the current and power output of the QBFB. With the exception of untreated Toray 060 electrodes, polarization curves were essentially linear over the range of conditions examined, permitting open-circuit voltage and area-specific resistance to be used as simple comparators. Acid-treatment of the Toray paper removes unnecessary overpotentials and

results in linear polarization curves. Baked SGL 10AA affords lower r_{pol} , the polarization resistance, than untreated SGL, both of which result in smaller polarization resistance, than etched or untreated Toray of equal thickness. The effect of electrode treatment correlates with observed hydrophilicity and appears to be correlated with accessible surface area. Pre-treated Nafion 212 outperforms other membranes due to its low resistance. The polarization resistance decreases and the short-circuit current density increases with increasing temperature and negolyte flow rate. The open-circuit potential increases with increasing Br_2 concentration and decreasing HBr concentration. These variations have enabled the cell to reach 1.0 W/cm^2 at 90% SOC. This is about 75% of the highest value reported in the literature for a vanadium redox flow battery⁶.

Acknowledgments. This research was supported partially by the US Department of Energy ARPA-E Award DE-AR0000348 and partially by the Harvard School of Engineering and Applied Sciences. We thank Roy G. Gordon for insightful discussions.

References:

1. M. Skyllas-Kazacos, M. H. Chakrabarti, S. A. Hajimolana, F. S. Mjalli, and M. Saleem, *J. Electrochem. Soc.*, **158**, R55 (2011).
2. A. Z. Weber, M. M. Mench, J. P. Meyers, P. N. Ross, J. T. Gostick, and Q. Liu, *J. Appl. Electrochem.*, **41**, 1137–1164 (2011).
3. B. R. Chalamala, T. Soundappan, G. R. Fisher, M. R. Anstey, V. V. Viswanathan, and M. L. Perry, *Proc. IEEE*, **102**, 976–999 (2014).
4. Z. Yang, J. Zhang, M. C. W. Kintner-Meyer, X. Lu, D. Choi, J. P. Lemmon, and J. Liu, *Chem. Rev.*, **111**, 3577–613 (2011).
5. T. V. Nguyen and R. F. Savinell, *Electrochemical Soc. Interface*, 54–56 (2010).
6. M. L. Perry, R. M. Darling, and R. Zaffou, *ECS Trans.*, **53**, 7–16 (2013).
7. B. Huskinson, M. P. Marshak, C. Suh, S. Er, M. R. Gerhardt, C. J. Galvin, X. Chen, A. Aspuru-Guzik, R. G. Gordon, and M. J. Aziz, *Nature*, **505**, 195–8 (2014).
8. B. Yang, L. Hooper-Burkhardt, F. Wang, G. K. Surya Prakash, and S. R. Narayanan, *J. Electrochem. Soc.*, **161**, A1371–A1380 (2014).
9. B. Huskinson, M. P. Marshak, M. R. Gerhardt, & M. J. Aziz, *ECS Trans.*, **61**, 27–30 (2014).
10. R. M. Darling and M. L. Perry, *J. Electrochem. Soc.*, **161**, A1381–A1387 (2014).
11. H. Zhou, H. Zhang, P. Zhao, and B. Yi, *Electrochim. Acta*, **51**, 6304–6312 (2006).
12. Q. H. Liu, G. M. Grim, A. B. Papandrew, A. Turhan, T. A. Zawodzinski, and M. M. Mench, *J. Electrochem. Soc.*, **159**, A1246–A1252 (2012).

13. M. Mastragostino and C. Gramellim, *Electrochim. Acta* (1985).

14. N. Pour, D. G. Kwabi, T. J. Carney, R. M. Darling, M. L. Perry, and Y. Shao-Horn, *J. Phys. Chem. C*, **119**, 5311–5318 (2015).

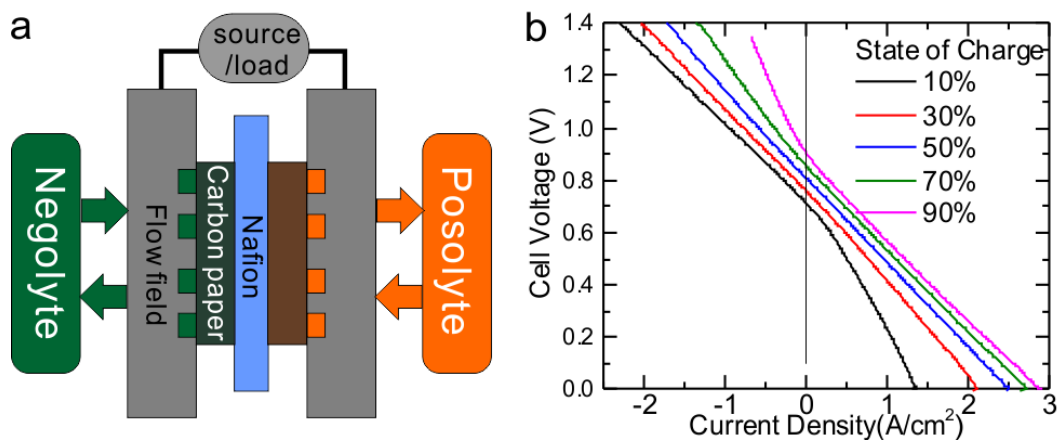


Figure 1. a. The cell configuration and **b.** the polarization curves at various stages of charge in the QBFB, for the base case detailed in the experimental session.

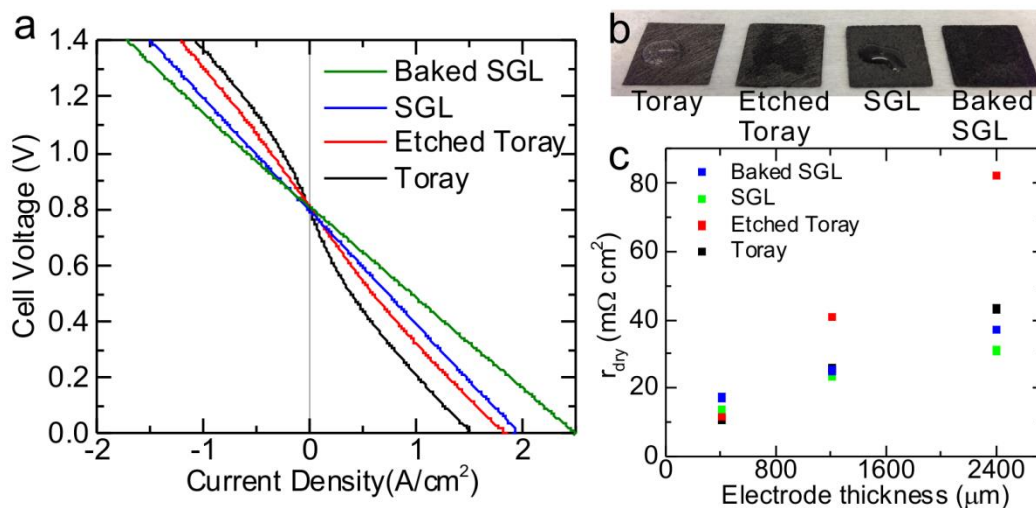


Figure 2. Comparison of porous carbon electrodes. **a.** Polarization curves at 50% SOC. **b.** A photo showing the wetting behavior of water drops on the carbon papers. **c.** r_{dry} vs. nominal electrode thickness for dry, compressed carbon electrodes.

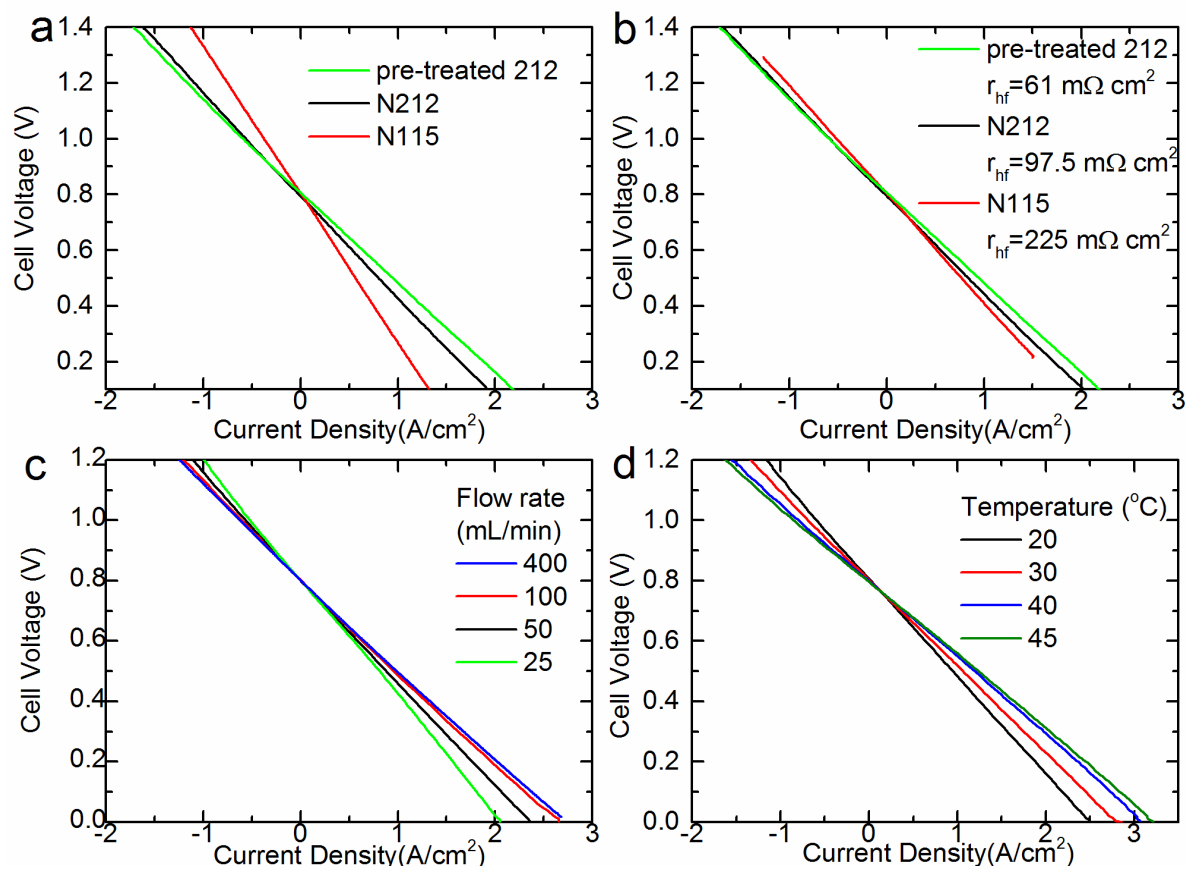


Figure 3. Polarization curves at 50% SOC **a.** and **b.** without and with IR_{hf} -correction when using different types of Nafion membrane; **c.** at different negolyte flow rates while the posolyte flow rate was kept at 200 mL/min.; **d.** at different cell temperatures.

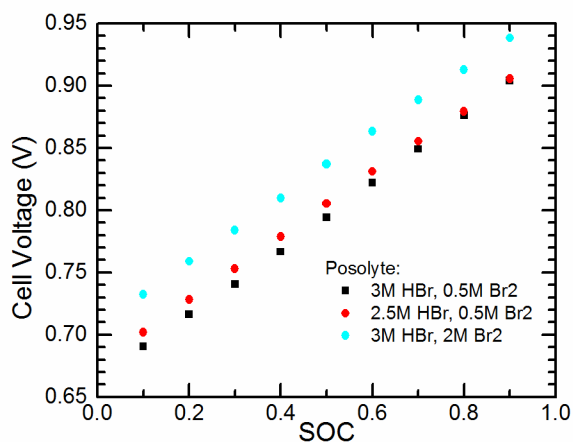


Figure 4. Cell open-circuit voltage vs. SOC with different posolyte contents with a negolyte consisting of 1 M AQDS and 1 M H_2SO_4 . Black squares represent base case. Red circles: cutting $[HBr]$ from 3.0 M to 2.5 M. Blue circles: raising $[Br_2]$ from 0.5 M to 2.0 M.

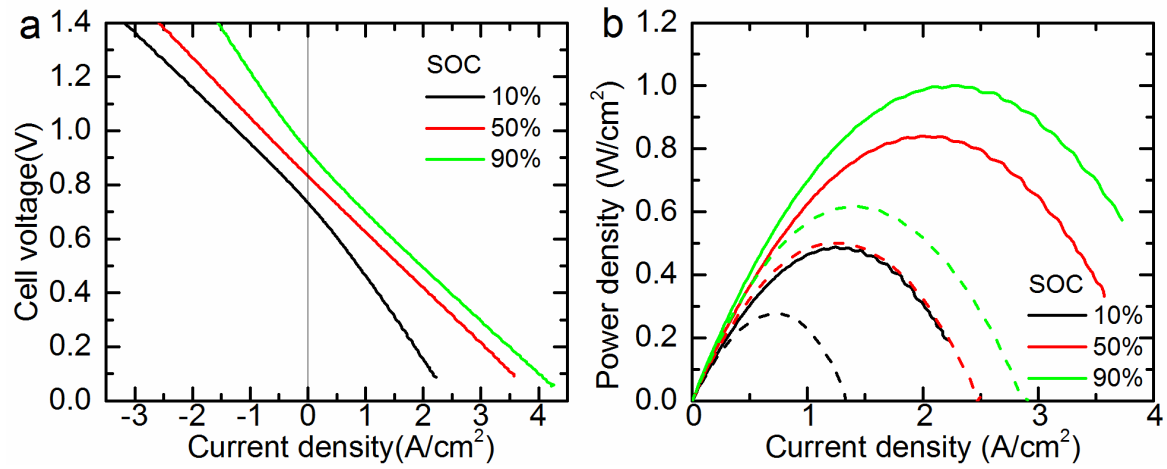


Figure 5. Modified cell performance at 10, 50 and 90% SOC: **a.** polarization curves; **b.** power density vs. current density. For comparison, the power density curves in the base case are plotted as the dashed lines in b.